

Electrical control over perpendicular magnetization switching driven by spin-orbit torques

X. Zhang, C. H. Wan,* Z. H. Yuan, Q. T. Zhang, H. Wu, L. Huang, W. J. Kong, C. Fang, U. Khan, and X. F. Han†
Institute of Physics, Chinese Academy of Sciences, Beijing National Laboratory for Condense Matter Physics, Beijing, 100190, China
(Dated: March 31, 2021)

Flexible control of magnetization switching by electrical manners is crucial for applications of spin-orbitronics. Besides of a switching current that is parallel to an applied field, a bias current that is normal to the switching current is introduced to tune the magnitude of effective damping-like and field-like torques and further to electrically control magnetization switching. Symmetrical and asymmetrical control over the critical switching current by the bias current with opposite polarities is both realized in Pt/Co/MgO and α -Ta/CoFeB/MgO systems, respectively. This research not only identifies the influences of field-like and damping-like torques on switching process but also demonstrates an electrical method to control it.

I. INTRODUCTION

Spin-orbitronics^{1,2}, aiming at current or voltage control of magnetization (M) via spin-orbit coupling (SOC) effect, has gradually manifested its charming prospect in nonvolatile magnetic storage and programmable spin-logic applications. Spin Hall effect (SHE) in heavy metals³⁻⁶ or topologic insulators⁷ and Rashba effect^{8,9} at the heavy metal/ferromagnetic metal interfaces are two broadly utilized effects to realize spin-orbitronics due to their large SOC strength. With the aid of magnetic field, SHE induced magnetization switching has already been realized in many systems comprising a magnetic layer (Co, CoFeB, NiFe) sandwiched by an oxide layer (AlO_x, MgO) and a heavy metal layer (Pt, β -Ta, W) with not only in-plane anisotropy^{10,11} but perpendicular anisotropy¹²⁻¹⁵. Recently, field-free magnetization switching via current has been also achieved in a wedged Ta/CoFeB/TaO_x¹⁶ or antiferromagnetic/ferromagnetic coupled perpendicular systems¹⁷⁻¹⁹.

In those perpendicular systems, current can generate via SHE effect a damping-like torque which balances effective torques from perpendicular anisotropy and in-plane bias field and consequently switches magnetization as it becomes large enough. In these previous researches, mainly spin Hall torque (along x axis) induced by one current (namely, switching current I along y axis) applied along the direction of an applied or effective magnetic field is taken into account while the influence of field-like torque (along y axis) on magnetic reversal process is rarely experimentally testified. Definition of coordinates is shown in Fig. 1(a).

Here, we introduced another current (namely, bias current I_B along x axis) to electrically control magnetization switching process (Fig. 1(a)). The damping-like and field-like torques of the bias current have the same symmetry with the field-like and damping-like torque of the switching current, respectively. Therefore, as shown below, the influences of both field-like torque and damping-like torque of the switching current on magnetization switching process become visible with tuning the magnitude of the bias current. Furthermore, the main features of aforementioned results can be well reproduced by a macrospin model which provides further understanding. This work can not only help to distill the influences of different kinds of torques on the switching process but also demonstrate a practical manner of controlling

SHE-driven magnetization switching process by electrically tuning the magnitude of effective damping-like and field-like torques.

II. EXPERIMENTAL METHOD

SiO₂//Ta(5)/Co₂₀Fe₆₀B₂₀(1)/MgO(2)/Pt(3) and SiO₂//Pt(5)/Co(0.8)/MgO(2)/Pt(3) (thickness in nanometer) stacks were provided by Singulus GmbH. They were magnetron-sputtered at room temperature. They have intrinsically in-plane anisotropy. After annealing at 400°C and 10⁻³ Pa for 1 h in a perpendicular field of 0.7 T could the stacks exhibit strong PMA. Raw films were then patterned by ultraviolet lithography and the following two-step argon ion etching into Hall bars with the size of the center squares being 20 μ m (Fig. 1(a)). Cu(10 nm)/Au(30 nm) electrodes were finally deposited to make contacts with four legs of Hall bars. After device microfabrication, the Hall bars were measured with two Keithley 2400 sourcemeters and Keithley 2182 voltmeter sourcing devices and measuring Hall voltages, respectively. Meanwhile, PPMS-9T (Quantum Design) provided magnetic fields with proper directions. The two Keithley 2400 sourcemeters first provided the current pulses to the Hall bar. One applied switching current along the y axis and the other applied bias current along the x axis to the sample with a duration time of 50 ms. Then the two Keithley 2400 stopped sourcing after the duration time. After waiting for 100 ms, one Keithley 2400 applied another current pulse of 1 mA along the y axis to the sample for 100 ms. At the end of this pulse, Keithley 2182 picked up the Hall voltage along the x axis. Then the Keithley 2400 was switched off. After 100 ms, the next round of destabilizing-measuring process was performed.

III. RESULTS AND DISCUSSION

A. Experiment

Two typical perpendicular systems Sub//Pt(5)/Co(0.8)/MgO(2)/Pt(3) (PCM for short) and Sub//Ta(5)/Co₂₀Fe₆₀B₂₀(1.0)/MgO(2)/Pt(3) (TFM) are used for comparison. Thickness is in nanometers. Here Ta is in

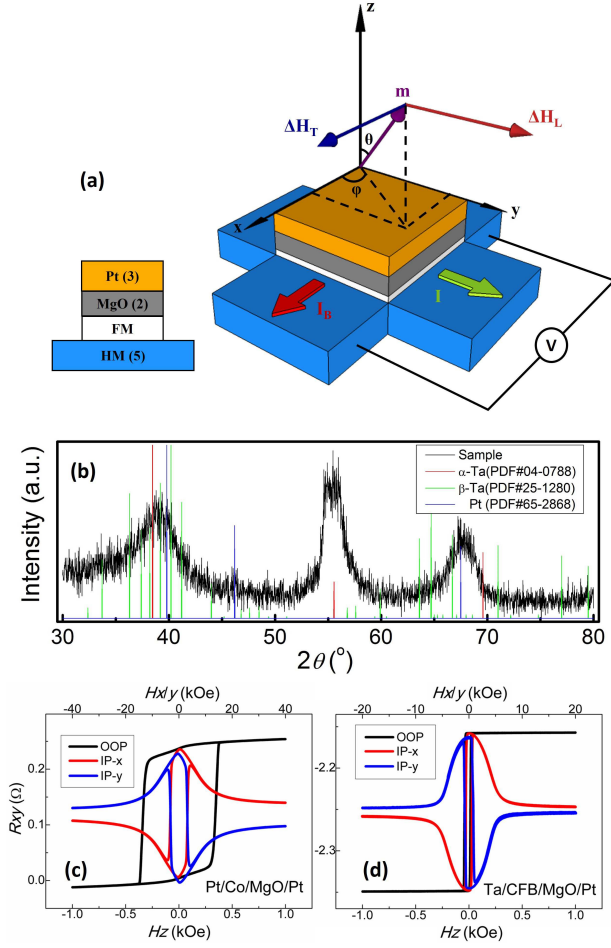


FIG. 1. (color online). (a) Sample structure of a Hall bar. (b) Glancing XRD pattern of Ta/Co₂₀Fe₆₀B₂₀/MgO/Pt stacks. (c) and (d) show H -dependence of Hall resistance of the PCM and TFM, respectively, as field is along $x/y/z$ axis. The Hall resistance $R_{xy} \equiv V_x/I_y$ in (c) and (d) is obtained as $I_y=1$ mA and $I_{Bx}=0$.

α -phase instead of β -phase (Fig. 1(b)). The strong peak at $2\theta=55.6^\circ$ can be only ascribed to (200) plane of α -Ta. Absence of the two main peaks at $2\theta=63.6^\circ$ and 64.7° corresponding to (631) and (413) planes of β -phase, respectively, indicates nonexistence of β -phase. The wide peak at $2\theta=39^\circ$ can be attributed to the merge of (110) plane of α -Ta and (111) plane of Pt. The other wide peak at $2\theta=68^\circ$ can be due to the merge of (211) plane of α -Ta and (220) plane of Pt.

M_0t of PCM and TFM measured by Vibration Sample Magnetometry is $125 \mu\text{emu}/\text{cm}^2$ and $145 \mu\text{emu}/\text{cm}^2$, respectively. M_0 and t is saturated magnetization and thickness of magnetic layer, respectively. Hall measurement demonstrates perpendicular magnetic anisotropy (PMA) of both systems. PCM shows higher PMA energy than TFM. Anisotropy field (H_{an}) of PCM and TFM is about 13.6 kOe and 5.8 kOe, respectively (Figs. 1(c) and 1(d)). Sophisticated harmonic lock-in technique^{20,21} is applied here to characterize spin-orbit torques of the above systems induced by applied current. The effective longitudinal field ΔH_L and effective

transverse field ΔH_T corresponding to damping-like torque and field-like torque, respectively, are shown in Fig. 1. Sample structure is also shown (Fig. 1(a)).

During measurement, current density ($j_y=j_{y0} \sin \omega t$) is applied along $+y$ axis. Magnetic field (H) is applied along x or y axis. Direction of H determines which torque can be detected. H_x and H_y are respectively used to measure current-induced field-like torque (or effective transverse field ΔH_T corresponding to the field-like torque) and damping-like torque (or effective longitudinal field ΔH_L corresponding to the damping-like torque). First and second harmonic Hall voltages along x axis ($V_x^\omega = V_{x0}^\omega \sin \omega t$ and $V_x^{2\omega} = V_{x0}^{2\omega} \cos 2\omega t$) are picked up to indirectly show direction of magnetization (\mathbf{M}) respective to the $+z$ axis and j_y -tuned \mathbf{M} change, accordingly. V_{x0}^ω and $V_{x0}^{2\omega}$ exhibit parabolic and linear field dependence as \mathbf{M} around $\pm z$, respectively. Especially, the $V_{x0}^{2\omega}$ vs. H curves (Fig. 2(b)) exhibit the same slopes at $\pm m_z$ as H is along y while they exhibit opposite slopes as H is along x (Fig. 2(d)). From the slopes as well as $\partial^2 V^\omega / \partial H^2$ (Figs. 2(a) and 2(c)) can we obtain ΔH_L along y axis and ΔH_T along x axis via $\Delta H_{L/T} = -2(\partial V^{2\omega} / \partial H_{y/x}) / (\partial^2 V^\omega / \partial H_{y/x}^2)$. Here ΔH_L parallel to $\sigma \times \mathbf{M}$ originates from spin Hall effect. ΔH_T parallel to σ originates from Rashba field as well as Osted field. The σ is the spin current density induced by the \mathbf{j}_y via $\sigma \propto \mathbf{j}_y \times \mathbf{z}$.

The $\Delta H_{L/T}$ shows linear dependence on applied current density j_y with zero intercepts as expected. Parameter $\beta_{L/T}$ defined as $d\Delta H_{L/T}/dj_y$ characterizes conversion efficiency from charge current to effective field. Here, $j_y = I/(wh_{\text{HM}})$. I is the switching current, w is the width of Hall bar (20 μm) and h_{HM} is the thickness of the heavy metal (5 nm). 1 mA of I thus corresponds to 1 MA/cm² of j_y . The shielding effect of the ferromagnetic layer and anti-oxidation layer is ignored. Thus, j_y and $\beta_{L/T}$ should be deemed as an upper and lower bound, respectively. The β_L is about -40 nm and +4 nm for PCM and TFM, respectively (Fig. 2(e)). Meanwhile, the β_T is about +1.2 nm and -4 nm for PCM and TFM, respectively (Fig. 2(f)). Especially, $\beta_{L/T}$ of α -Ta and Pt has opposite signs. The $\beta_{L/T}$ of Pt is reported in the order of 1 $\mu\text{m}-1$ nm^{9,10,13,20,22} in different systems. Our value is closer to that of Liu¹³ and Fan¹⁰. Besides, $|\beta_{L,\text{Pt}}| \gg |\beta_{T,\text{Pt}}|$, consistent with the results of Liu¹³. The $\beta_{L/T}$ of Ta in Ta/CoFeB/MgO system is thoroughly researched by Kim²¹. It is in the order of 2-20 nm, depending on thickness of Ta and CoFeB. Besides, their results show $\beta_{T,\text{Ta}}$ can be comparable and even larger than $\beta_{L,\text{Ta}}$. Our measured values are within their range and $|\beta_{L,\text{Ta}}|$ is equal to $|\beta_{T,\text{Ta}}|$. However, the β_L of α -Ta is smaller than that of β -Ta²¹. Ratio of β_T/β_L for Pt and α -Ta is -0.03 and -1, respectively. Field-like torque can be nearly neglected in the PCM while it cannot be ignored in the TFM, which provides us a couple of ideal systems to research the influence of field-like torque and damping-like torque on switching behavior of perpendicular films. The reason why field-like torque is insignificant and significant in PCM and TFM system respectively, we think, is that the two systems may have different interfacial potentials due to different work functions of Pt (5.3 eV), Co (4.4 eV), Fe (4.3 eV), and Ta (4.1 eV)^{23,24} as elaborated in Ref. [25].

In the following, we will use the PCM with $\beta_T/\beta_L=-0.03$ and the TFM with $\beta_T/\beta_L=-1$ to study the influence of I_B on

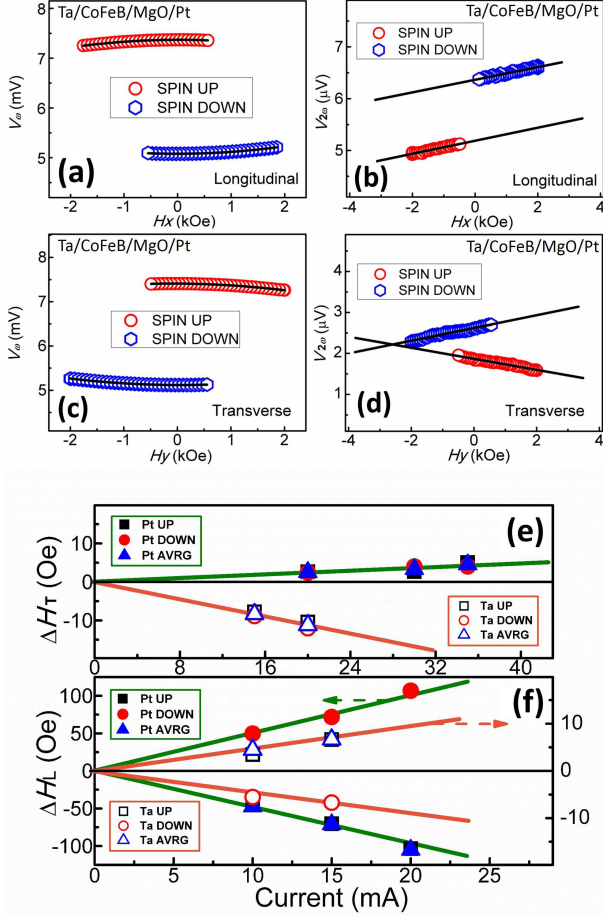


FIG. 2. (color online). The H_y dependence of (a) V^{ω} and (b) $V^{2\omega}$ and the H_x dependence of (c) V^{ω} and (d) $V^{2\omega}$ in TFM. (e) and (f) shows, respectively, the current dependence of ΔH_T and ΔH_L in both TFM and PCM films. Their linear fittings with zero intercept are also shown. As measuring the effective fields induced by the switching current, we applied no bias current. FM and HM denote ferromagnetic and heavy metal, respectively.

switching behaviors and introduce the underneath mechanism based on a macrospin model. I and H_y are applied along y . I_B is applied along x . As $I_B=0$, \mathbf{M} can be switched back and forth between spin-up state and spin-down state (Fig. 3) by scanning I under nonzero H_y . Due to opposite spin Hall angle, switching direction is opposite for PCM and TFM with the same measurement setup. For example, switching direction for TFM and PCM is clockwise and anticlockwise, respectively, at positive H_y . Sign reversal of H_y leads to reversal of the switching direction. Fig. 3 also shows nearly a full magnetization switching can be realized as $H_y=0.3$ kOe for TFM. In this condition, critical switching current (I_C) is 63.5 mA. Meanwhile, the I_C for PCM is about 80 mA as $H_y=0.7$ kOe. These results manifest α -Ta can also function as a high efficiency converter from charge current to spin current besides of Pt and β -Ta.

As shown in Figs. 4(a) and 4(b) elevated I_B can significantly reduce the I_C in the PCM system. For example, $I_C=88$

mA as $I_B=0$ mA while $I_C=73$ mA as $I_B=50$ mA. I_C decreases by 17%. Meanwhile, positive and negative I_B leads to nearly the same amount of reduction, no matter the sign of H_y as shown by the parabolic fitting lines in Figs. 4(c) and 4(d). This I_B -induced decrease in I_C can be ascribed to the damping-like torque from I_B as shown in the theoretical part below. It is worthy of accentuating that the damping-like torque of I_B shares the similar symmetry with the field-like torque of I and thus a large field-like torque of I could also in principle reduce the I_C .

Certainly, I_B will heat magnetic films as well and in principle reduce the effective H_{an} , which could also reduce I_C . However, our experiment shows that I_C varies little as changing duration time of I_B from 50 ms to 1 s, which indicates that thermal effect is at least not dominating factor in determining I_C here.

On the other hand, TFM system manifests a different response to I_B with different symmetry in comparison with the PCM counterpart. As shown in Figs. 5(a) and 5(c) for $H_y=+100$ Oe and the transition from down-state to up-state, I_C is reduced by about 67% under $I_B=40$ mA while it is only reduced by 20% under $I_B=-40$ mA. In contrast, for $H_y=-100$ Oe and the transition from up-state to down-state (Figs. 5(b) and 5(d)), besides of the opposite switching direction, the effect of I_B on I_C is also reversed, i.e. I_C decreased only by about 5% under $I_B=40$ mA while it decreased remarkably by 53% under $I_B=-40$ mA. Here, the asymmetric response of I_C to positive and negative I_B cannot be interpreted by damping-like torque induced by I_B or heating effect as shown in the case of PCM. Instead, field-like torque of I_B is a key contributor to the asymmetry as shown below.

B. Macrospin model

In order to interpret the different response of PCM and TFM to I_B , we have turned to a macrospin model (more details in Appendix). The magnetic energy includes uniaxial anisotropy energy $K \sin^2 \theta$ and Zeeman energy $-H_y M_0 \sin \theta \sin \varphi$ where θ and φ is the polar angle between \mathbf{M} and the $+z$ axis and the azimuthal angle between in-plane projection of \mathbf{M} and the $+x$ axis, respectively (Fig. 1(a)). I and I_B provide both a damping-like torque and a field-like torque on \mathbf{M} with efficiency characterized by β_T/β_L . We use parameter a in unit of $H_{an} \equiv 2K/\mu_0 M_0$ to denote the damping-like torque provided by I , parameter c to denote the ratio of I_B/I and parameter b to denote the ratio of β_T/β_L . Actually, c reflects the angle of total current density with respect to the direction of magnetic field. As I and I_B are both applied, torque equilibrium condition requires satisfaction of Eq. (1).

$$0 = \vec{m} \times \vec{H}_{eff} + a\vec{m} \times (-\hat{e}_x) \times \vec{m} + ab\vec{m} \times (-\hat{e}_x) + ac\vec{m} \times \hat{e}_y \times \vec{m} + abc\vec{m} \times \hat{e}_y \quad (1)$$

Here $\mathbf{H}_{eff} = -\nabla_M E$, $\mathbf{m} \equiv \mathbf{M}/M_0$, $E \equiv K \sin^2 \theta - \mu_0 M_0 H_y \sin \theta \cos \varphi$, \mathbf{e}_x and \mathbf{e}_y is a unit vector along the x and y axes, respectively. The 2nd and 3rd term in the RHS

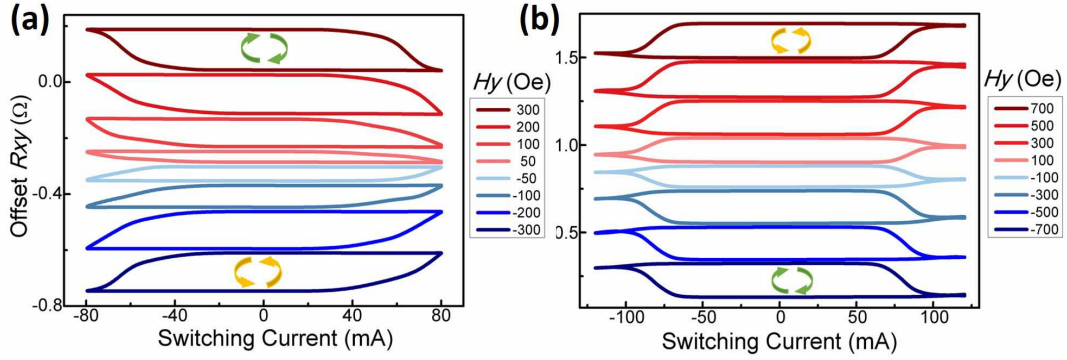


FIG. 3. (color online). The dependence of R_{xy} on switching current (I) in (a) TFM and (b) PCM systems under different H_y .

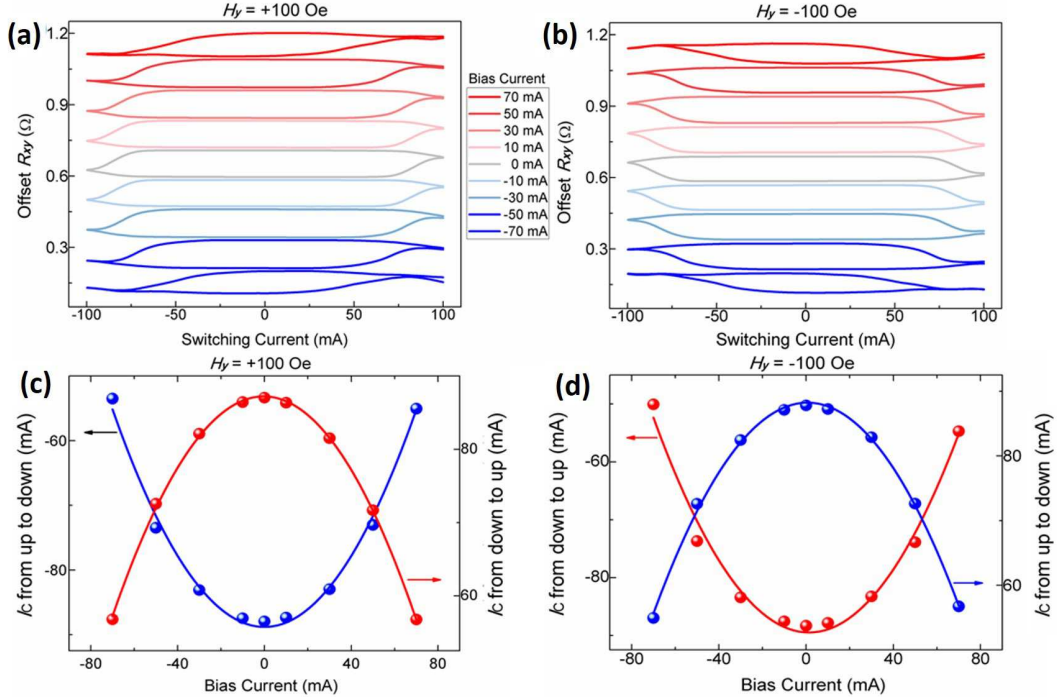


FIG. 4. (color online). The switching current dependence of R_{xy} of the PCM under different bias current as (a) $H_y=100$ Oe and (b) -100 Oe and the dependence of I_C on I_B as (c) $H_y=100$ Oe and (d) -100 Oe. Red and blue dots in (c) and (d) show, respectively, the I_C of transitions from down-state to up-state and from up-state to down-state. The dependence of I_C on I_B in (c) and (d) could be well reproduced by parabolic fittings.

of Equation (1) is damping-like and field-like torque from I while the 4th and 5th term is damping-like and field-like

torque from I_B , respectively. Equation (1) can be further reduced as scalar equations. Equation (2) is one of them.

$$\sin \theta \cos \theta - \frac{[a^2(b^2 + 1)(c^2 + 1) + h_y^2 - 2abch_y]}{h_y - a \cos \theta - abc} \cos \theta \sin \varphi + \frac{ah_y(1 + \cos^2 \theta)}{h_y - a \cos \theta - abc} \sin \varphi = 0 \quad (2)$$

If $I_B=0$ and $b=0$, $\sin \theta \cos \theta - h_y \cos \theta \sin \varphi + a \sin \varphi = 0$, which shares the similar form as derived by Liu¹³ and Yan²⁶. Here $h_y \equiv H_y/H_{an}$. Comparing Eq. (2) with the simplified

one as $I_B=0$ and $b=0$, we can see that introduction of I_B leads to an effective h_y^{eff} and an effective damping-like torque a^{eff}

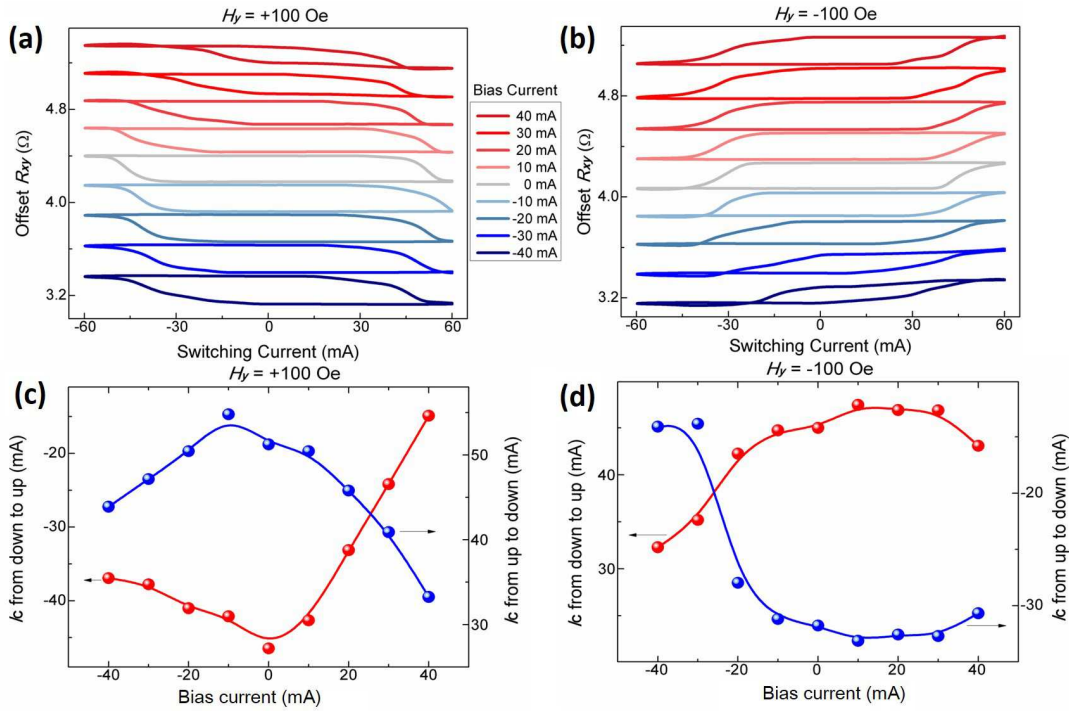


FIG. 5. (color online). The switching current dependence of R_{xy} of the TFM under different bias current as (a) $H_y=+100$ Oe and (b) -100 Oe and the dependence of I_C on I_B as (c) $H_y=+100$ Oe and (d) -100 Oe.

as expressed in Equation (3).

$$h_y^{eff} = \frac{[a^2(b^2 + 1)(c^2 + 1) + h_y^2 - 2abch_y]}{h_y - a \cos \theta - abc} \quad (3a)$$

$$a^{eff} = \frac{ah_y(1 + \cos^2 \theta)}{h_y - a \cos \theta - abc} \quad (3b)$$

Simulated results according to Eq. (1) are shown in Fig. 6 where $\tau_c \propto I_C$ is the critical damping-like torque of I . As $c=0$, a nonzero b can significantly reduce critical switching current (I_C), regardless of its sign (Fig. 6(g)). I_C decreases by 5.8% and 42% as $b=\pm 1$ and $b=\pm 3.6^{21}$, respectively, compared with the I_C as $b=0$. This trend is consistent with the result in the PCM sample in which the damping-like torque of I_B can mimic the influence of the field-like torque of I . Though it cannot reverse \mathbf{M} directly, large Rashba effect can still help to effectively reduce I_C .

As $b=0$, bias current ($c \neq 0$) can notably decrease I_C and the amount of the reduction in I_C does not depend on polarity of c (Figs. 6(a) and 6(b)), which manifests similar characteristics with the switching behaviors of the PCM sample. As $b=-1$ and $h_y=0.4$ (Fig. 6(c)), $c=0.3$ and $c=-0.3$ will result in asymmetric decrease in I_C . Here $c=-0.3$ is more effective in reducing I_C . However, as $h_y=-0.4$ (Fig. 6(d)), I_C reduces more in the case of $c=+0.3$. These characteristics (Figs. 6(c) and 6(d)) will reproduce the results of the TFM sample in Figs. 5(a) and 5(b). Figs. 6(e) and 6(f) shows the I_B dependence of I_C as $b=0$ and $b=-1$, respectively. The former indeed predicts a parabolic dependence as observed in Figs. 4(c) and 4(d) while the latter

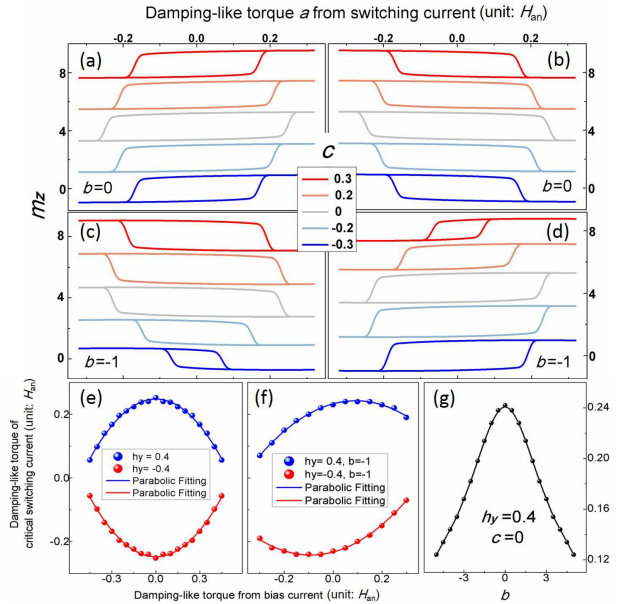


FIG. 6. (color online). Dependence of m_z on damping-like torque of switching current a (in unit of H_{an}) for different c , as (a) $h_y=0.4$, (b) $h_y=0.4$ with $b=0$ and (c) $h_y=0.4$, (d) $h_y=0.4$ with $b=-1$. (e) and (f) τ_c as a function of damping-like torque of I_B under $h_y=\pm 0.4$ as $b=0$ and $b=-1$, respectively. Here τ_c is obtained by the transition from spin-down to spin-up state. (g) τ_c as a function of b as $c=0$ and $h_y=0.4$.

also predicts a linear dependence besides of the parabolic one, which qualitatively reproduces the results in Figs. 5(c) and 5(d). It is worth bearing that field-like torque and damping-like torque are both indispensable to realize the asymmetry reduction of I_C under opposite I_B . Fig. 5 also indirectly manifests that the two types of torque both play important roles in magnetization switching process of the TFM system.

Other Pt/Co/MgO and Ta/CoFeB/MgO samples have exhibited similar switching symmetries. Noteworthy, though we demonstrate the switching behaviors with aid of an applied field, the switching performance controlled by I_B will be still achievable in principle if the applied field is replaced by an effective field from exchange coupling.

IV. SUMMARY

Current induced torques of Pt and α -Ta, including damping-like torque and field-like torque, have been characterized by second-harmonic technique as $\beta_{L, Pt} = -40$ nm, $\beta_{L, Ta} = +4$ nm, $\beta_{T, Pt} = +1.2$ nm and $\beta_{T, Ta} = -4$ nm. Current can generate much larger field-like torque in α -Ta than in Pt. Current-induced magnetization switching has also been realized in the α -Ta system, indicating its high enough spin-orbit coupling strength and shedding light on its potential use in spin-orbitronics. Field-like torque, though incapable of switching \mathbf{M} directly in our case, plays crucial role in reducing I_C .

I_B results in different influences on switching behaviors for the TFM and PCM systems. Opposite I_B equally decreases I_C in PCM while it asymmetrically influences the I_C in TFM system. Furthermore this asymmetry originates from the field-like torque of I_B and can be adjusted by polarity of H_y . Our work not only brings to light the influence of damping-like and field-like torques of switching current and bias current on switching but also experimentally demonstrates an electrical manner (via bias current) to symmetrically or asymmetrically control the switching, which could advance the development of spin-logic applications in which control of the switching process via electrical methods is crucial and beneficial.

ACKNOWLEDGMENTS

This work was supported by the 863 Plan Project of Ministry of Science and Technology (MOST) (Grant No. 2014AA032904), the MOST National Key Scientific Instrument and Equipment Development Projects [Grant No. 2011YQ120053], the National Natural Science Foundation of China (NSFC) [Grant No. 11434014, 51229101, 11404382] and the Strategic Priority Research Program (B) of the Chinese Academy of Sciences (CAS) [Grant No. XDB07030200].

Appendix: DETAILS OF MACROSPIN MODEL

The schematic structure of the Pt/Co/MgO or Ta/CoFeB/MgO is shown in Fig. 1(a). An applied field H_y and the switching current (I) are along the $+y$ axis. The bias current (I_B) is along the $+x$ axis. The ratio of I_B/I is defined as a parameter c which actually reflects the angle between the direction of total current density with that of the applied field. Easy axis of the perpendicular systems (PCM or TFM) is along the z axis. Therefore the total energy (E) is $K \sin^2 \theta - \mu_0 M_0 H_y \sin \theta \sin \varphi$ with K anisotropy energy, M_0 saturation magnetization and μ_0 permeability of vacuum. This energy drives an effective field $\mathbf{H}_{\text{eff}} = -\nabla_{\mathbf{M}} E$. Here we use a macrospin model for simplicity and therefore only θ and φ are variable with the M_0 being a constant. $H_{\theta, \text{eff}} = -H_{\text{an}} \sin \theta \cos \theta + H_y \cos \theta \sin \varphi$ and $H_{\varphi, \text{eff}} = H_y \cos \varphi$. $H_{\text{an}} \equiv 2K/\mu_0 M_0$. $H_{\theta, \text{eff}}$ and $H_{\varphi, \text{eff}}$ are two orthogonal components of \mathbf{H}_{eff} . As the currents I and I_B are both applied, magnetization direction will be modulated due to the damping-like and field-like torques originated from the I and I_B . The damping-like torque of a unit of \mathbf{M} induced by the I via spin Hall effect is defined as a parameter a which is proportional to the spin Hall angle and along the x axis. Then the damping-like torque induced by the I_B is ac which is however along the y axis. As shown in the maintext, $\beta_{L(T)}$ is defined as the effective field correspond to the damping (field)-like torque induced by an unit of I . Here we further define b as β_T/β_L . Thus field-like torque induced by the I via Rashba effect as well as Ostered mechanism is ab and along the y axis. In contrast, the field-like torque induced by the I_B is abc and along the x axis. It is very important that the direction of the field-like torque induced by the I is the same as that of the damping-like torque induced by the I_B . They are both along the y axis. The final state of the system is determined by the following LLG equation (A.1).

$$\begin{aligned} -\frac{1}{\gamma} \frac{d\vec{M}}{M_0 dt} = & -\alpha \vec{M} \times \frac{d\vec{M}}{M_0 dt} + \frac{\vec{M}}{M_0} \times \vec{H}_{\text{eff}} \\ & + a \frac{\vec{M}}{M_0} \times (-\hat{e}_x) \times \frac{\vec{M}}{M_0} + ab \frac{\vec{M}}{M_0} \times (-\hat{e}_x) \\ & + ac \frac{\vec{M}}{M_0} \times \hat{e}_y \times \frac{\vec{M}}{M_0} + abc \frac{\vec{M}}{M_0} \times \hat{e}_y \end{aligned} \quad (\text{A.1})$$

In the first line of Equation (A.1), γ and α are gyromagnetic ratio and damping constant, respectively. The quantity \hat{e}_x and \hat{e}_y is unit vector along the x and y axis, respectively. The 1st and 2nd term in the second line is damping-like and field-like torque induced by the switching current (I), respectively. The 1st and 2nd term in the third line is damping-like and field-like torque induced by the bias current (I_B), respectively. At the steady state, $d\vec{M}/M_0 dt = 0$. Thus we arrive at Equation (A.2).

$$\begin{aligned} 0 = & \vec{m} \times \vec{H}_{\text{eff}} \\ & + a \vec{m} \times (-\hat{e}_x) \times \vec{m} + ab \vec{m} \times (-\hat{e}_x) \\ & + ac \vec{m} \times \hat{e}_y \times \vec{m} + abc \vec{m} \times \hat{e}_y \end{aligned} \quad (\text{A.2})$$

Here we have replaced \mathbf{M}/M_0 with \mathbf{m} . Equation (A.2) gives

the scalar equations (A.3) which is also shown in the main text.

$$H_y \cos \varphi - a \cos \theta \cos \varphi - ab \sin \varphi + ac \cos \theta \sin \varphi - abc \cos \varphi = 0 \quad (\text{A.3a})$$

$$H_y \cos \theta \sin^2 \varphi - H_{an} \sin \theta \cos \theta \sin \varphi - a \sin^2 \varphi + ab \cos \theta \sin \varphi \cos \varphi - ac \sin \varphi \cos \varphi - abc \cos \theta \sin^2 \varphi = 0 \quad (\text{A.3b})$$

As $c=b=0$, Equation (A.3) is reduced as Equation (A.4)

$$(H_y - a \cos \theta) \cos \varphi = 0 \quad (\text{A.4a})$$

$$\sin \varphi (H_y \cos \theta \sin \varphi - H_{an} \sin \theta \cos \theta - a \sin \varphi) = 0 \quad (\text{A.4b})$$

One possible solution as well as the final physically meaningful solution of Equation (A.4) is further reduced as Equation (A.5)

$$\cos \varphi = 0 \quad (\text{A.5a})$$

$$H_{an} \sin \theta \cos \theta - H_y \cos \theta \sin \varphi + a \sin \varphi = 0 \quad (\text{A.5b})$$

This solution shares the similar form with that derived in Ref.[13], which demonstrates the rationality of our deriva-

tions.

In general case, Equation (A.3) can be transformed as Equation (A.6).

$$\cos \varphi = \frac{(ab - ac \cos \theta) \sin \varphi}{H_y - a \cos \theta - abc} \quad (\text{A.6a})$$

$$H_{an} \sin \theta \cos \theta - \frac{[(H_y - abc)^2 + a^2(b^2 + c^2 + 1)]}{H_y - a \cos \theta - abc} \cos \theta \sin \varphi + \frac{aH_y(1 + \cos^2 \theta)}{H_y - a \cos \theta - abc} \sin \varphi = 0 \quad (\text{A.6b})$$

Comparing Equation (A.5b) and (A.6b), we find that the introduction of I_B actually updates the H_y with an effective field of $[(H_y - abc)^2 + a^2(b^2 + c^2 + 1)]/(H_y - a \cos \theta - abc)$ and updates the a with an effective torque of $aH_y(1 + \cos^2 \theta)/(H_y - a \cos \theta - abc)$.

As $c=0$, the effective field becomes $[H_y^2 + a^2(b^2 + 1)]/(H_y - a \cos \theta)$. A nonzero b can make the effective field larger, which is very beneficial for higher efficient switching. As $b=0$, the effective field becomes $[H_y^2 + a^2(c^2 + 1)]/(H_y - a \cos \theta)$. Therefore, the introduction of the bias current (or

nonzero c regardless of its polarity) can also increase the effective field. Besides, the field-like torque of the switching current (ab) in the former case functions a similar role with the damping-like torque of the bias current (ac) in the latter case. Only as $b \neq 0$ can c with opposite sign asymmetrically influence the effective field. It is also worth noting that the H_y is still indispensable for magnetization switching because a zero H_y will also lead to a zero effective torque. The numerical results regarding the solutions of Equation (A.3) are shown in the Fig. 6 in the main text and not shown here.

* Email: wancaihua@iphy.ac.cn

† Email: xfhan@iphy.ac.cn

- ¹ T. Kuschel and G. Reiss, *Nature Nanotech* **10**, 22 (2014).
- ² A. Manchon, *Nat Phys* **10**, 340 (2014).
- ³ M. I. D'Yakonov and V. I. Perel', *JETP Letters* **13**, 467 (1971).
- ⁴ J. E. Hirsch, *Phys. Rev. Lett.* **83**, 1834 (1999).
- ⁵ S. Zhang, *Phys. Rev. Lett.* **85**, 393 (2000).
- ⁶ J. Sinova, S. O. Valenzuela, J. Wunderlich, C. H. Back, and T. Jungwirth, *Rev. Mod. Phys.* **87**, 1213 (2015).
- ⁷ Y. Fan, P. Upadhyaya, X. Kou, M. Lang, S. Takei, Z. Wang, J. Tang, L. He, L.-T. Chang, M. Montazeri, G. Yu, W. Jiang, T. Nie, R. N. Schwartz, Y. Tserkovnyak, and K. L. Wang, *Nature Materials* **13**, 699 (2014).
- ⁸ Y. A. Bychkov and E. I. Rashba, *JETP Letters* **39**, 66 (1984).
- ⁹ I. M. Miron, G. Gaudin, S. Auffret, B. Rodmacq, A. Schuhl, S. Pizzini, J. Vogel, and P. Gambardella, *Nature Materials* (2010).
- ¹⁰ X. Fan, J. Wu, Y. Chen, M. J. Jerry, H. Zhang, and J. Q. Xiao, *Nature Communications* **4**, 1799 (2013).
- ¹¹ L. Liu, C.-F. Pai, Y. Li, H. W. Tseng, D. C. Ralph, and R. A. Buhrman, *Science* **336**, 555 (2012).
- ¹² I. M. Miron, K. Garello, G. Gaudin, P.-J. Zermatten, M. V. Costache, S. Auffret, S. Bandiera, B. Rodmacq, A. Schuhl, and P. Gambardella, *Nature (London)* **476**, 189 (2011).
- ¹³ L. Liu, O. J. Lee, T. J. Gudmundsen, D. C. Ralph, and R. A. Buhrman, *Phys. Rev. Lett.* **109** (2012).
- ¹⁴ C.-F. Pai, L. Liu, Y. Li, H. W. Tseng, D. C. Ralph, and R. A. Buhrman, *Appl. Phys. Lett.* **101**, 122404 (2012).
- ¹⁵ X. Qiu, K. Narayanapillai, Y. Wu, P. Deorani, D.-H. Yang, W.-S. Noh, J.-H. Park, K.-J. Lee, H.-W. Lee, and H. Yang, *Nature Nanotech* **10**, 333 (2015).
- ¹⁶ G. Yu, P. Upadhyaya, Y. Fan, J. G. Alzate, W. Jiang, K. L. Wong, S. Takei, S. A. Bender, L.-T. Chang, Y. Jiang, M. Lang, J. Tang, Y. Wang, Y. Tserkovnyak, P. K. Amiri, and K. L. Wang, *Nature Nanotech* **9**, 548 (2014).
- ¹⁷ S. Fukami, C. Zhang, S. DuttaGupta, A. Kurenkov, and H. Ohno, *Nature Materials* **15**, 535 (2016).
- ¹⁸ A. van den Brink, G. Vermeij, A. Solignac, J. Koo, J. T. Kohlhepp, H. J. M. Swagten, and B. Koopmans, *Nature Communications* **7**, 10854 (2016).
- ¹⁹ Y.-C. Lau, D. Betto, K. Rode, J. Coey, and P. Stamenov, (2015), arXiv:1511.05773 .
- ²⁰ U. H. Pi, K. W. Kim, J. Y. Bae, S. C. Lee, Y. J. Cho, K. S. Kim, and S. Seo, *Appl. Phys. Lett.* **97**, 162507 (2010).
- ²¹ J. Kim, J. Sinha, M. Hayashi, M. Yamanouchi, S. Fukami, T. Suzuki, S. Mitani, and H. Ohno, *Nature Materials* **12**, 240 (2012).
- ²² X. Fan, H. Celik, J. Wu, C. Ni, K.-J. Lee, V. O. Lorenz, and J. Q. Xiao, *Nature Communications* **5** (2014).
- ²³ H. B. Michaelson, *J. Appl. Phys.* **48**, 4729 (1977).
- ²⁴ H. L. Skriver and N. M. Rosengaard, *Phys. Rev. B* **46**, 7157 (1992).
- ²⁵ S. E. Barnes, J. Ieda, and S. Maekawa, *Sci. Rep.* **4** (2014).
- ²⁶ S. Yan and Y. B. Bazaliy, *Phys. Rev. B* **91** (2015).